



Evaluating the Impact of Inclined Cutoff-Wall to Control Seawater Intrusion in Heterogeneous Coastal Aquifers

Sobhy R. Emara¹ · Tamer A. Gado¹ · Bakenaz A. Zeidan¹ ·
Asaad M. Armanuos¹

Received: 30 July 2023 / Accepted: 4 October 2023 / Published online: 16 October 2023
© The Author(s) 2023

Abstract

Subsurface physical barriers have been effectively used to mitigate seawater intrusion (SWI). Traditionally, the primary emphasis in both numerical studies and practical implementations has been on vertical barriers. The current research aims to explore the dynamics of SWI under various cutoff-wall inclination angles and depths, as well as aquifer heterogeneity using both experimental and numerical simulations. The impact of aquifer characteristics was assessed by utilizing a low hydraulic conductivity (K) aquifer (case L), a high hydraulic conductivity aquifer (case H), and two stratified aquifers. The stratified aquifers were created by grouping different hydraulic conductivity layers into two cases: high K above low K (case H/L) and low K above high K (case L/H). The model simulations covered seven different cutoff-wall inclination angles: 45.0°, 63.4°, 76.0°, 90.0°, 104.0°, 116.6°, and 135.0°. The maximum repulsion ratio of SWI wedge length was observed at an inclination angle of 76.0° for cutoff-wall depth ratios up to 0.623. However, as the depth ratio increased to 0.811, the maximum repulsion ratio shifted to an angle of 63.4° for all aquifers studied. At an inclined cutoff depth ratio of 0.811, the cutoff-wall inclination angle of 45.0° had the most significant impact on the saltwater wedge area. This results in SWI area reductions of 74.9%, 79.8%, 74.7%, and 62.6% for case L, case H, case H/L, and case L/H, respectively. This study provides practical insights into the prevention of SWI. Nevertheless, a thorough cost–benefit analysis is necessary to assess the feasibility of constructing inclined cutoff-walls.

Keywords Coastal aquifers · Heterogeneity · Saltwater intrusion · Groundwater remediation · Inclined cutoff-wall

✉ Asaad M. Armanuos
asaad.matter@f-eng.tanta.edu.eg

Sobhy R. Emara
sobhy_emara39@f-eng.tanta.edu.eg

Tamer A. Gado
tamer.gado@f-eng.tanta.edu.eg

Bakenaz A. Zeidan
b.zeidan@f-eng.tanta.edu.eg

¹ Irrigation and Hydraulics Engineering Department, Faculty of Engineering, Tanta University, Tanta, Egypt

1 Introduction

Seawater intrusion (SWI), or contamination of coastal groundwater with seawater, poses a main challenge for coastal regions across the world. This is particularly pronounced in cases where groundwater (GW) serves as the primary source of freshwater supply. The adverse impacts of SWI are primarily attributed to the over-extraction of groundwater (Werner et al. 2013).

To hinder saltwater intrusion and maintain groundwater quality in coastal zones, researchers have proposed various engineering solutions. These include optimizing the layout of pumping well (Liu et al. 2019; Ranjbar et al. 2020; Fan et al. 2020) employing positive hydraulic barriers such as artificial recharge through infiltration or injection (Hussain et al. 2016; Motallebian et al. 2019; Armanuos et al. 2020a), using negative hydraulic barriers like pumping inland saltwater (Javadi et al. 2015; Mehdizadeh et al. 2019), and implementing underground physical barriers (Kaleris and Ziogas 2013; Abd-Elaty et al. 2019; Armanuos et al. 2019, 2020b).

Numerical simulations and laboratory experiments have been employed in numerous studies to assess the effectiveness of subsurface barriers in managing saltwater intrusion. These studies have aimed to evaluate the performance of underground barriers concerning their ability to limit the ingress of saltwater into freshwater aquifers while preserving water quality. Additionally, They have examined factors including the location, design, and construction of these subsurface barriers, and their impact on the hydrogeological conditions of aquifers (Li et al. 2018; Takahashi et al. 2018; Armanuos et al. 2019; Wu et al. 2020; Gao et al. 2021; Abdoulhalik et al. 2022a).

Li et al. (2018) used the FEFLOW model and a physical sandbox model to examine the effectiveness of underground barriers in preventing SWI. They found that barriers with limited permeability effectively prevented intrusion. Chang et al. (2019) proposed the use of underground dams with the lowest efficient height to prevent SWI. They evaluated the environmental impact and efficiency of this approach using fresh GW discharge and observed that as the distance of the dam from the coastline increased, both the minimum efficient height and maximum fresh GW flow also increased. Lee et al. (2019) conducted hydraulic model tests to measure the equilibrium interface of seawater with subsurface constraints. They found that an increase in groundwater levels caused by subsurface impediments such as a seawall, enhanced the pressure gradient and groundwater flow rate, thereby slowing down saltwater intrusion into coastal aquifers. Wu et al. (2020) utilized SEAWAT to investigate the impact of impervious barriers on preventing saltwater intrusion and found that cutoff-walls were most effective when located close to the coastline and that fully penetrating barriers outperformed cutoff-walls and underground dams.

Kaleris and Ziogas (2013) used the SUTRA code to simulate the impact of cutoff-walls on SWI and the protection of groundwater extraction near the coast. They found that the effectiveness of cutoff-walls can be affected by various factors, including the wall's depth, distance from the shoreline, groundwater velocity, mixing intensity, and wall conductivity. They also determined the maximum safe abstraction discharge before and after wall installation. Jamshidzadeh and Ghasemzadeh (2017) developed a 2D finite difference model to assess the impact of cutoff-walls on saltwater intrusion and found that cutoff-walls had a significant impact on preventing saltwater intrusion. Takahashi et al. (2018) investigated the influence of dispersivity on the efficiency of seawater removal in a laboratory-scale cutoff-wall test. They discovered that when low

dispersivity was used, the remaining seawater was eliminated more rapidly compared to the experimental results, whereas higher dispersivity resulted in a prolonged time for the removal of the remaining seawater.

The effectiveness of employing physical underground barriers to manage SWI in the Biscayne Aquifer in the United States was assessed by Abd-Elaty et al. (2019). Their findings indicated that physical underground barriers can effectively limit SWI, with cutoff-walls being more effective in repelling saltwater compared to underground dams. Zheng et al. (2021) used a simulation–optimization approach to investigate the optimal placement of cutoff-walls for preventing saltwater intrusion. They concluded that this technology provides a reliable technique for determining the ideal location of cutoff-walls. Zheng et al. (2022) used both numerical simulations and laboratory experiments to study the movement and desalination of saltwater following the installation of a cutoff-wall. They found that a deeper cutoff-wall can lead to more effective removal of residual seawater. Chang et al. (2022) combined computer simulations with laboratory experimental tests to study the effect of cutoff-walls on downstream seawater in coastal aquifers. Their results showed that cutoff-walls could cause the seawater wedge to extend further inland, resulting in a wider mixing zone, reduced freshwater discharge, and increased saltwater intrusion into coastal groundwater. However, they observed that cutoff-walls are more efficient in aquifers with low hydraulic gradients when positioned closer to the coastline, thus reducing SWI in coastal aquifers without increasing construction costs.

The SEAWAT model was utilized by Armanuos et al. (2020a, b) to examine the impact of cutoff-walls on saltwater intrusion in sloping bed coastal aquifers, revealing that raising the depth ratios of cutoff-walls pushed the seawater interface towards the shoreline, thereby increasing the retreading percentage. In different bed sloping scenarios, barrier walls exceeding a depth ratio of 0.4 yielded higher repulsion values, particularly when placed deeper towards the seawater side, effectively repelling SWI. Using a combination of experiments and computer simulations, Abdoulhalik et al. (2022a, b) assessed the effect of cutoff-walls on seawater upconing, concluding that these walls did not significantly delay saltwater upconing in the tested aquifer settings. They also emphasized that the efficiency of cutoff-walls depended greatly on their design and placement, with walls located closer to the pumped well proving more effective in enhancing the efficiency of freshwater extraction, particularly for deeper wells. The study highlighted that cut-off barriers do not always need to reach the depth of the pumping well to be effective, a crucial consideration from both construction and economic perspectives. Abd-Elaty et al. (2022) explored the effectiveness of inclined subsurface barriers in mitigating SWI in different scenarios, finding that cut-off walls outperformed subsurface dams in reducing SWI, with the most significant positive effect achieved when using a slope of 1/4.

Zheng T, Zheng X, Chang Q et al. (2021) were pioneers in uncovering how saltwater can be effectively removed in the presence of subsurface dams. They also investigated the influence of dam structure and aquifer characteristics on the efficiency of saltwater removal upstream of the dam. The study revealed that in scenarios with high-concentration gradients, a crucial mechanism for saltwater removal involves the lower-concentration mixing zone, acting as a significant pathway for saltwater to traverse over the subsurface dam and reach the saltwater edge. This sheds light on the ongoing dissemination of saltwater and its progression towards the aquifer's edge.

Luyun et al. (2011) investigated the impact of recharge wells and cutoff-walls in preventing saltwater intrusion. They concluded that deeper cutoff-walls positioned closer to the coastline are more effective at repelling saltwater, whereas seawater intrusion increases when the cutoff-wall is located farther from the initial toe site. Armanuos et al. (2019)

investigated the mitigation of SWI using cutoff-walls, recharge wells, or a combination of both, employing the SEAWAT code. They found that the combined approach of freshwater injection and physical barriers was the most effective in pushing back seawater, resulting in higher repulsion ratio values compared to using a cutoff-wall or freshwater injection alone.

Groundwater movement along coastal regions is affected by geological heterogeneity in the underground structure, mainly attributed to spatial variations in hydraulic conductivity. This phenomenon plays a crucial role in shaping the saltwater-freshwater interface, determining the location and rate of freshwater discharge into the sea (Houben et al. 2018). The impact of heterogeneity on pollutant transport in aquifer can vary depending on the level of heterogeneity (Werner et al. 2013). Dagan and Zeitoun (1998) used the sharp interface method to examine how aquifer variations affect the freshwater-saltwater interface. Lu et al. (2013) conducted laboratory research on the effects of aquifer stratification levels on saltwater intrusion, discovering that homogeneous aquifers had larger saltwater wedge extents compared to layered aquifers. Ahmed et al. (2022) utilized a combination of numerical modeling and laboratory experiments to examine saltwater intrusion in complex and heterogeneous aquifers. Their findings revealed unique gradient changes in the seawater interface across regions with different hydraulic conductivity. They also found that refraction affected the mixing zone, leading to increased dispersion when transitioning between higher to lower permeability regions. The study observed relatively impermeable regions near saltwater boundaries in the aquifer, resulting in a narrower horizontal saltwater wedge but a more extensive vertical spread. Abdoulhalik and Ahmed (2017) investigated the effectiveness of cutoff-walls in preventing seawater intrusion into layered, heterogeneous coastal aquifers using both numerical simulation and laboratory tests. They found that the walls were more effective on steeper slopes than shallower ones, but the soil layering reduced their overall effectiveness. The specific arrangement of layers affected freshwater velocity at the wall's opening and flow dynamics to varying degrees.

A comprehensive analysis of existing literature reveals that previous research on controlling saltwater intrusion (SWI) primarily focused on using physical barriers in homogeneous medium, although such conditions were relatively rare. The investigation into the impact of inclined cutoff-walls on saltwater removal was limited to homogenous conditions (Abd-Elaty et al. 2022). Nevertheless, to the best of the authors' knowledge, the utilization of inclined cutoff-walls to manage saltwater intrusion in diverse coastal aquifers has not been previously explored. Therefore, the current study aims to examine the effectiveness of inclined cutoff-walls in mitigating saltwater intrusion in different types of soil formations, employing a combination of experimental tests and numerical simulations. Additionally, the study seeks to analyze the dynamics of SWI under various cutoff-wall inclination angles, depths, and aquifer characteristics in transient conditions. Laboratory experiments were conducted using a 2D sandbox, while numerical simulations were performed using the SEAWAT code.

2 Materials and Methods

Seven different cutoff-wall inclination angles were considered: 45.0°, 63.4°, 76.0°, 90.0°, 104.0°, 116.6°, and 135.0°. These were tested in four distinct aquifer settings, including a low-conductivity aquifer (Case L), and a high-conductivity aquifer (Case H), and two stratified aquifers. The stratified aquifers were formed by grouping two layers with different hydraulic conductivity (K), resulting in two cases high K above low K (Case H/L) and low

K above high K (Case L/H). Using a vertical 2D cross-section domain, several scenarios with different configurations were created. To assess the efficacy of saltwater removal after the installation of inclined cutoff-wall, the reduction rate of the saltwater wedge length (R_L) was calculated. The dimensionless cutoff-wall depth (H_c^*) was utilized to determine the most effective cutoff-wall dimensions.

2.1 Experimental Methods

The practice of simulating the behavior and impact of saltwater intrusion has traditionally relied on the use of scaled-down or physical models (e.g., Christensen and Evans 1974; Brakefield 2008; Luyun et al. 2011; Werner et al. 2013; Armanuos et al. 2019; Hussain et al. 2019). These models are valuable tools for studying and visualizing the interactions between fluids with different properties within the same domain. In this study, the experimental tests were conducted in the Irrigation and Hydraulics Engineering Laboratory at the Faculty of Engineering, Tanta University, Egypt.

The research was conducted using a transparent acrylic tank, with dimensions of 114 cm in length, 28 cm in height, and 8 cm in width. This tank served as a laboratory sandbox to simulate a 2D cross-section of an unconfined coastal aquifer (Fig. A-1). The tank was divided into three sections, arranged from right to left: saltwater, porous medium, and freshwater. Both the freshwater and saltwater sections measured 12 cm in length, while the porous medium section spanned 90 cm in length. To isolate the reservoirs, a fine mesh screen was employed, allowing water to pass through while effectively preventing the porous material from crossing over.

The sand underwent thorough blending before being packed and was gently compressed after packing (Gao et al. 2021). During the packing process, clamps were employed to prevent expansion and maintain a constant width of the sand tank (Armanuos et al. 2019). The study evaluated two different homogenous aquifers and two layered aquifers (Fig. A-2). The high permeability aquifer was created using sand with an average particle size of 1700 μm and a hydraulic conductivity of 0.700 cm/sec, while the low permeability aquifer was constructed using sand with an average particle size of 1180 μm and a hydraulic conductivity of 0.377 cm/sec. The hydraulic conductivity (K) of each sand type was determined using Darcy's law, as illustrated in Section 2.2.

Freshwater was sourced from the tap. Before commencing the experiments, a solution of 250 L of saltwater was prepared by dissolving commercially available salt (sodium chloride) in freshwater, achieving a concentration of 36,000 mg/L. The freshwater density was measured at 1,000 g/L using a densitometer, while seawater's density was recorded at 1,025 g/L. To distinguish between the two types of water, the seawater was tinted red using a dye concentration of 20 g per 40 L. Two tanks were used to deliver saltwater and freshwater at a steady flow rate through saltwater and freshwater feed pipelines, respectively. Adjustable drainage pipes were utilized to regulate the levels of freshwater and saltwater as needed.

2.2 Experimental Procedure

Freshwater was initially filled into the side reservoirs and the porous medium tank at the start of each experiment. The drainage pipes were adjusted to control the levels of freshwater and saltwater in the reservoirs. The saltwater level on the right-hand side was set at 26.5 cm, while the inland groundwater head on the left-hand side was established at 27.5 cm. Water level fluctuations during the experiments were estimated to be minimal, around

1.0 mm. The flow from the freshwater reservoir to the saltwater reservoir was driven by a hydraulic gradient ($J=1.11\%$) that existed between the two heads. In the experimental sandbox tank, Darcy's law was applied to determine the average hydraulic conductivity (K) of different types of sand. This involved analyzing the measured freshwater flow rates from the drainage pipes and the hydraulic gradient. The estimated hydraulic conductivity for the low K and high K aquifers was determined to be 0.377 and 0.700 cm/sec, respectively. Following the flow measurement, a shut-off wall was installed to isolate the saltwater reservoir from the central porous medium tank. Subsequently, the dyed saltwater was introduced into the saltwater reservoir to replace the freshwater. The barrier between the aquifer medium and the saltwater reservoir was removed to initiate the saltwater intrusion process in the aquifer medium. The experiments were conducted once the density measurements had stabilized.

Three different cutoff-wall inclination angles were experimentally examined: 63.4° (equivalent to a slope of 1/2 on the saltwater side), 90.0° (vertical), and 116.6° (a slope of 1/2 on the landside). These angles were tested in four distinct aquifer configurations, as illustrated in Tables A-1 and A-2. For each aquifer setup, five tests were conducted for each cutoff-wall inclination angle, including simulating saltwater intrusion under natural conditions (without any barriers), inserting an impermeable sheet as a cutoff-wall at a depth of 10 cm, increasing the cutoff-wall depth to 15 cm, increasing it further to 20 cm, and finally increasing it to 25 cm. Prior to progressing to the next experiment in each scenario, the SWI wedge was allowed to reach a steady state. The toe position of the SWI wedge was monitored at ten-minute intervals until it reached a steady state for each test.

2.3 Numerical Model (SEAWAT)

A numerical model was developed to interpret and build upon the experimental findings. The SEAWAT code has been utilized extensively in addressing saltwater intrusion challenges within sandbox experimental simulation (Abdoulhalik et al. 2022b). SEAWAT was utilized in the current study to investigate the impact of the inclined cutoff-wall on the removal of saltwater intrusion in heterogeneous soil formations. The model examined the mechanisms of saline water intrusion and retraction both before and after the installation of the inclined cutoff-wall.

To numerically investigate the influence of an inclined cutoff-wall on SWI, four aquifers were simulated, comprising two homogenous aquifers and two different stratified aquifers. The first homogenous aquifer represents low-conductivity soil media (Case L) with a hydraulic conductivity (K_L) of 0.377 cm/sec. The second homogenous aquifer represents high-conductivity soil media (Case H) with a hydraulic conductivity (K_H) of 0.700 cm/sec. The stratified aquifers were composed of two layers with different hydraulic conductivity (K), as shown in Fig. A-2. The longitudinal dispersivity of the porous media (α_L) was set at 15 mm, a common value in laboratory-scale studies (Abarca and Clement 2009; Sun et al. 2019; Chang et al. 2020; Armanuos et al. 2020a; Vats et al. 2020). The transverse dispersivity (α_T) was set to be 10% of α_L , consistent with previous research (Walther et al. 2017; Armanuos et al. 2019).

The SEAWAT simulation area comprises a vertical 2D section with dimensions of $90.0\text{ cm} \times 30.0\text{ cm}$, which is uniformly discretized into a finite-difference mesh with quadratic elements of size $\Delta x \times \Delta z = 0.5\text{ cm} \times 0.5\text{ cm}$ (Fig. A-3). To ensure numerical stability, the grid spacing and dispersivity must satisfy the Péclet number criterion (Voss and Souza 1987). Péclet number ($Pe_m \approx \Delta x / \alpha_l$) is a dimensionless value that quantifies the ratio of local advective transport to local diffusion and dispersive transport, where α_l is the longitudinal

dispersivity of the porous media. In this study, both the dispersivity value and the grid spatial discretization satisfy the Péclet number criterion ($Pe_m = 3.33 < 4.0$), ensuring sufficient numerical stability.

In the case of stratified aquifers, each of the two layers had a thickness of 15 cm. During the simulation, only one variable was altered at a time. A total of 116 sets of simulations (4 aquifers \times 29 simulations/aquifer) were carried out according to the model parameters specified in Table A-2.

The salt concentration (C_s) was set to 36,000 mg/L at the right-hand side as the saltwater boundary, maintaining a constant head (h_s) of 26.50 cm. On the left side, the freshwater salt concentration (C_f) was fixed at 0.0 mg/L. The densities of saltwater and freshwater were set at 1,025 g/L and 1,000 g/L, respectively. A hydraulic gradient of 0.0111 was applied to the system by adjusting the freshwater level (h_f) to 27.5 cm, to establish a 1.0 cm difference in the GW head. This value falls within the range of hydraulic gradients typically employed in prior laboratory-scale research of a similar nature (e.g., Chang and Clement 2012; Abdoulhalik and Ahmed 2017). Figure A-3 illustrates the boundary conditions of the numerical simulations, where the cutoff-wall (black bar) is located 20.0 cm away from the saline water boundary. The wall depth is denoted as H_c .

As a baseline scenario, simulations were conducted for the four aquifers without the cutoff-wall to establish an initial stable saltwater-freshwater interface. The simulation procedures for both the baseline and the management scenarios were nearly identical. To incorporate the cutoff-wall into the SEAWAT simulation, the cells encompassed by the wall were set as inactive (Luyun et al. 2009; Gao et al. 2021).

2.4 Evaluation Method

The saltwater wedge repulsion ratio (R_L) was established to assess the efficacy of removing residual saline water following the installation of the cutoff-wall (Luyun et al. 2011; Armanuos et al. 2019; Motallebian et al. 2019; Gao et al. 2021). The index was calculated as follows:

$$R_L = \frac{L_i - L}{L_i} \quad (1)$$

where L_i is the initial length of the residual saltwater wedge, measured from the saltwater boundary on the right side, and L is the length of the residual saline water wedge after the cutoff-wall installation, also measured from the saltwater boundary on the right side. To track the position of the toe, measurements were taken every ten minutes until the SWI wedge reached a steady-state condition, defined as when the variation in SWI penetration length was less than 1.0 mm for 30.0 min. The toe location was determined using the 50% saltwater salinity isoline (18,000 mg/L), which is also used to identify the geometry of the freshwater-saltwater interface (Ahmed et al. 2022).

3 Results and Discussions

3.1 Experimental Results

Figures 1, A-4 and A-5 illustrate steady-state SWI wedge images for four different aquifer configurations, considering cutoff-wall angles θ of 63.4°, 90.0°, and 116.6°, respectively, obtained for varying inclined cutoff-wall depths of 10.0, 15.0, 20.0, and 25.0 cm. Notably, as

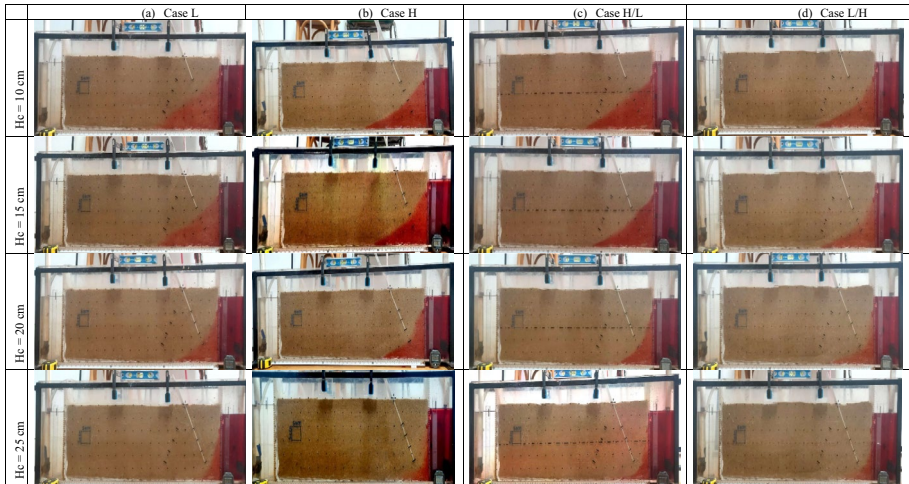


Fig. 1 Experimental results of saltwater intrusion wedge for $\theta = 63.43^\circ$, for various aquifer cases **a** Case L, **b** Case H, **c** Case H/L, and **d** Case L/H, for four various presented cutoff-wall depths

the penetration depth of the inclined cutoff-wall increased, the gap between the cutoff-wall and the saltwater wedge decreased, causing the groundwater to flow beneath the cutoff-wall, thus pushing the SWI back towards the sea. For an inclination angle of 63.4° , the saltwater intrusion wedge penetration length declined rapidly from 40.0 cm to 15.0 cm within 290 min and from 36.1 cm to 16.6 cm within 270 min in Case H and Case L/H, respectively. This observation highlights the more pronounced effect of a 63.4° inclination angle in reducing SWI wedge penetration lengths compared to an angle of 90.0° and 116.6° .

3.2 Numerical Results

Figures A-6 to A-8 and 2 display the results of steady-state numerical analysis for different types of aquifers, including homogenous low conductivity, homogenous high conductivity, stratified high conductivity layer above a low conductivity layer, and stratified low conductivity layer above a high conductivity layer. These analyses encompass the base case (with no barriers) and scenarios involving cutoff-wall depths of 10, 15, 20, and 25 cm at various cutoff-wall inclination angles (45.0° , 63.4° , 76.0° , 90.0° , 104.0° , 116.6° , and 135.0°) for each case.

In the base case, the steady-state saltwater intrusion lengths are 38.99, 39.87, 41.76, and 36.38 cm for Case L, Case H, Case H/L, and Case L/H, respectively (Table A-3). In each aquifer case, once the steady-state was achieved, the process of saltwater removal began by the installation of the cutoff-wall at a depth of 10 cm at initial cutoff-wall inclination angle of $\theta = 45.0^\circ$. The inclined cutoff-wall depth was subsequently increased to 15.0, 20.0, and 25.0 cm, allowing the saltwater wedge to reach a steady-state condition at each step. These same steps were systematically repeated for all investigated inclination angles.

As the increasing cutoff-wall depth, the SWI wedge gradually retreats towards the sea in all the investigated cases. For cutoff-wall depths up to 20 cm, the cutoff-wall inclination angle $\theta = 76.0^\circ$ had the largest impact on the SWI wedge length, causing it to decrease from 38.99, 39.87, 41.76, and 36.38 cm (base case) to 25.70, 25.62, 23.10, and 27.16 cm for Case L, Case H, Case H/L, and Case L/H, respectively, at an inclined cutoff depth of 20

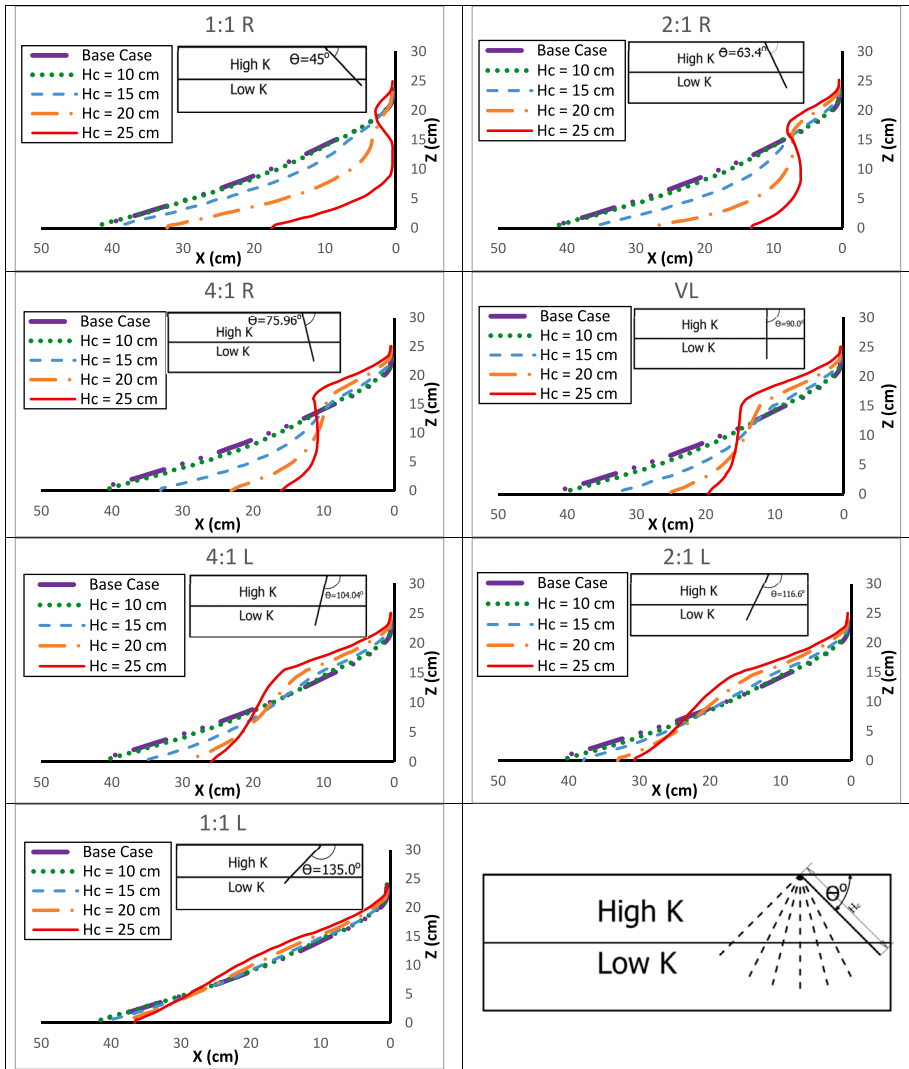


Fig. 2 Steady-state numerical results of saltwater intrusion wedge for cutoff-wall depths of 10.0, 15.0, 20.0, and 25.0 cm at cutoff-wall inclination angles of 45.0°, 63.4°, 76.0°, 90.0°, 104.0°, 116.6°, and 135.0° for a stratified aquifer with a high conductivity layer above a low conductivity layer (Case H/L)

cm. However, for a cutoff-wall depth of 25 cm, the cutoff-wall inclination angle $\theta = 63.4^\circ$ had the greatest impact on the saltwater wedge length. At this depth, the SWI wedge length decreases to 15.52, 15.28, 13.22, and 17.20 cm for Case L, Case H, Case H/L, and Case L/H, respectively.

In the base case, the areas of the SWI wedges at the steady state are 316.98, 372.90, 310.41, and 254.03 cm² for Case L, Case H, Case H/L, and Case L/H, respectively (Fig. 3). The cutoff-wall inclination angle of 45.0° has the most significant impact, shrinking the area of the SWI wedge from the base case values of 316.98, 372.90, 310.41, and 254.03 cm² to 79.54, 75.19, 79.74, and 95.0 cm² for Case L, Case H, Case H/L, and Case L/H, respectively, at an inclined cutoff depth of 25 cm.

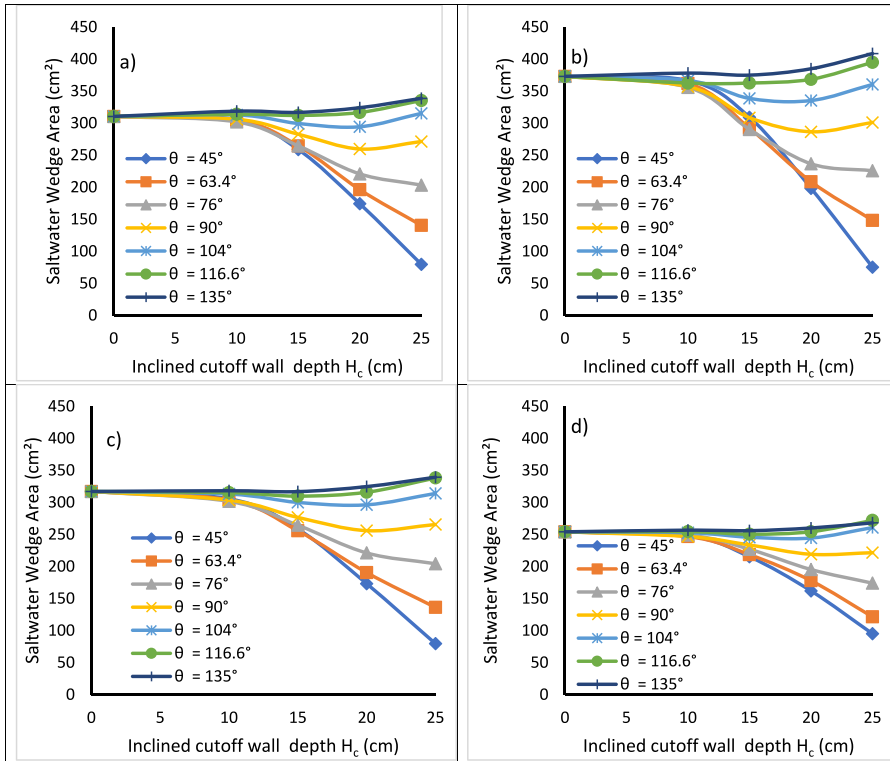


Fig. 3 Steady-state numerical results of SWI wedge area for cutoff-wall depths of 10.0, 15.0, 20.0, and 25.0 cm at cutoff-wall inclination angles of 45.0° , 63.4° , 76.0° , 90.0° , 104.0° , 116.6° , and 135.0° for Case L (a), Case H (b), Case H/L (c), and Case L/H (d)

3.3 Experimental and Numerical Transient SWI Length

The study investigated the impact of SWI in coastal aquifers and how different aquifer characteristics and varying cutoff-wall angles influence the length of the SWI wedge. The research examined the saltwater intrusion length in four distinct aquifers, designated as Case L, Case H, Case H/L, and Case L/H, by comparing the length of the saltwater intrusion wedge using both experimental and numerical techniques. The outcomes of these comparisons are represented in three Figs. A-9, A-10 and A-11, corresponding to various cutoff-wall inclination angles (θ) of 63.4° , 90.0° , and 116.4° respectively. For the four various aquifers studied, the transient saltwater penetration length obtained through numerical analysis closely matched the experimental results.

The study found that, in the four aquifers under consideration, the saltwater wedge reached a steady state after different durations of time. Specifically, it took 235, 160, 190, and 160 min for the SWI wedges to reach their respective steady states. The steady-state lengths of SWI wedge were 38.0 cm, 40.0 cm, 40.0 cm, and 36.1 cm in Case L, Case H, Case H/L, and Case L/H, respectively.

For the cutoff-wall inclination angle of 116.6° , the results illustrated that increasing the depth of the inclined cutoff-wall did not have a significant impact on reducing the saltwater intrusion length. There was only a slight decrease in the penetration length

as the depth of the inclined cutoff-wall increased up to 25.0 cm. Specifically, the salt-water wedge penetration length decreased from 38.0, 40.0, 40.0, and 36.2 cm to 30.7, 30.7, 30.2, and 30.8 cm for Case L, Case H, Case H/L, and Case L/H, respectively.

3.4 Impact of the Cutoff-Wall Inclination Angle θ

The study investigated the impact of cutoff-wall inclination angles on the repulsion ratio of saltwater intrusion in heterogeneous aquifers by examining seven inclination angles (45.0° , 63.4° , 76.0° , 90.0° , 104.0° , 116.6° , and 135.0°) within four different aquifer settings: a homogenous low conductivity aquifer (Case L), a homogenous high conductivity aquifer (Case H), a stratified aquifer with a high conductivity layer over a low conductivity layer (Case H/L), and a stratified aquifer with a low conductivity layer over a high conductivity layer (Case L/H). The results are presented in Fig. 4,

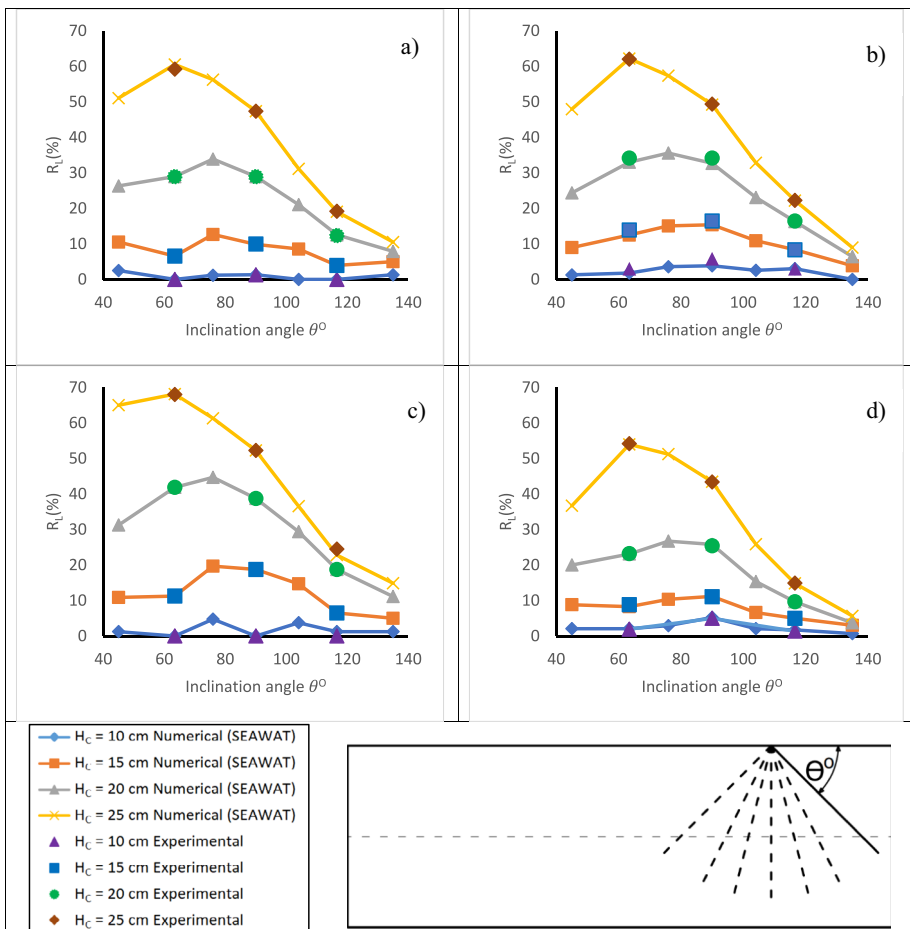


Fig. 4 Impact of the cutoff-wall inclination angle θ on the repulsion ratio of SWI for Case L (a), Case H (b), Case H/L (c), and Case L/H (d)

illustrating the effect of cutoff-wall inclination angles on the repulsion ratio of SWI for four diverse cutoff-wall depths (10.0 cm, 15.0 cm, 20.0 cm, and 25.0 cm) in the four examined aquifer settings. Additionally, the study compared the repulsion ratio results obtained from experimental and numerical simulations. For the four various aquifers studied, the numerical repulsion ratio of SWI agreed well with the experimental results.

Figure 4 illustrates that as the cutoff-wall inclination angle increases from 45.0° to 63.4° , the repulsion ratio of saltwater intrusion increases, showing an increase in the repulsion ratio from 51.05%, 47.95%, 65.0%, and 36.69% to 59.21%, 62.03%, 68.00%, and 54.14% for Case L, Case H, Case H/L, and Case L/H, respectively, when the depth of the inclined cutoff-wall is 25.0 cm. However, when the inclination angle is further increased beyond 63.4° up to 135.0° , there is a significant decrease in the SWI repulsion ratio, with the repulsion ratio decreasing from 59.21%, 62.03%, 68.00%, and 54.14% to 10.53%, 8.97%, 14.88%, and 5.66% for Case L, Case H, Case H/L, and Case L/H, respectively, at an inclined cutoff-wall depth of 25.0 cm.

The study's results indicate that across all investigated aquifers, the least saltwater intrusion penetration occurred when the inclination angle of the cutoff-wall, θ , was set at 76.0° , corresponding to a cutoff-wall slope of 1/4 at the seaside. This effect was observed for cutoff-wall depths up to 20.0 cm. However, when the cutoff-wall depth was increased to 25.0 cm, the minimum values for saltwater intrusion penetration length were observed when the inclination angle was set at 63.4° , corresponding to a cutoff-wall slope of 1/2 at the seaside.

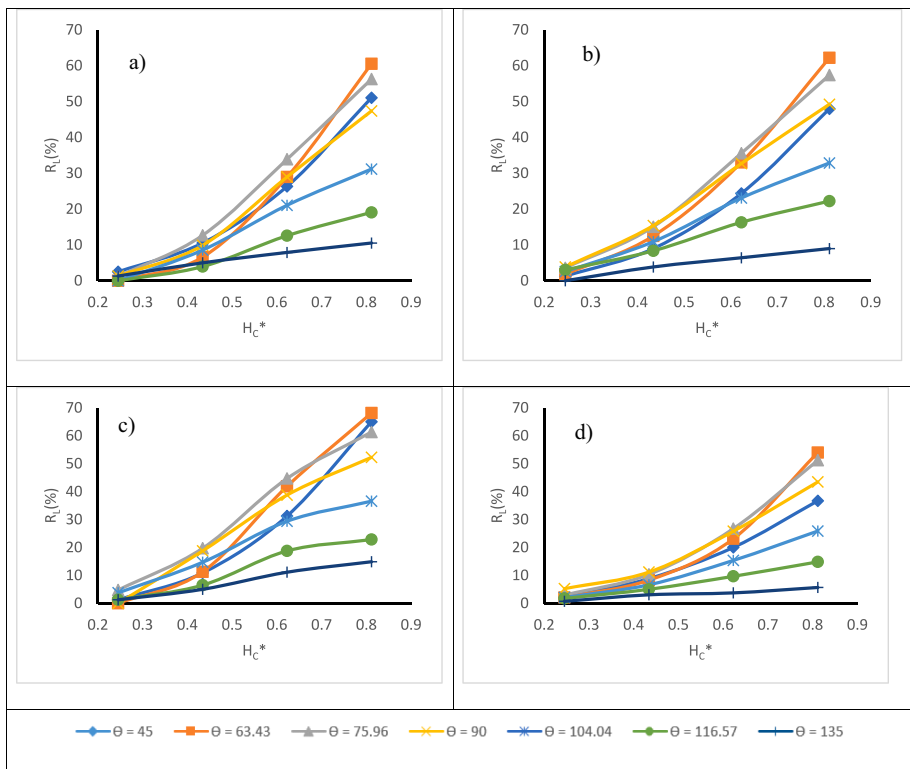


Fig. 5 Impact of the inclined cutoff-wall dimensionless depth H_c^* on the numerical repulsion-ratio of SWI for Case L (a), Case H (b), Case H/L (c), and Case L/H (d)

3.5 Impact of the Inclined Cutoff-Wall Dimensionless Depth H_c^*

Figure 5 illustrates the relationship between the inclined cutoff-wall depth (measured as a dimensionless number, H_c^*) and the repulsion ratio of SWI in four different aquifers. The repulsion ratio of SWI was calculated for seven different cutoff-wall inclination angles (45.0° , 63.4° , 76.0° , 90.0° , 104.0° , 116.6° , and 135.0°) within the four examined aquifers. The results reveal that the repulsion ratio of SWI increases as the inclined cutoff-wall depth increases, signifying that a greater depth of the inclined cutoff-wall is more effective in preventing saltwater intrusion into the aquifer.

The study found that the highest values of the repulsion ratio for saltwater intrusion were achieved when the inclination angle of the cutoff-wall was set at 76.0° for dimensionless depths up to 0.623 in all four investigated aquifers. However, as the dimensionless depth increased to 0.811, the maximum values for the SWI repulsion ratio were attained with an inclination angle of 63.4° (Figs. A-12 to A-15).

4 Conclusions

This study explored the impact of inclined cutoff-walls on the removal of residual saline water from multi-layered, unconfined coastal aquifers. To comprehensively investigate this phenomenon, a dual approach was employed, combining physical sandbox experiments with numerical SEAWAT models. The research aimed to shed light on how various factors, including cutoff-wall angle, depth, and aquifer properties, influence saltwater intrusion dynamics under both steady-state and transient conditions. Four distinct aquifer configurations were examined, including two homogeneous and two layered aquifers. Diverse scenarios were meticulously examined, each involving different cutoff-wall inclination angles and penetration depths. Impressively, the numerical simulation results regarding saltwater intrusion length closely aligned with the experimental data.

In the baseline scenario, the steady-state saltwater intrusion area varied among cases: 316.98 cm^2 for Case L, 372.90 cm^2 for Case H, 310.41 cm^2 for Case H/L, and 254.03 cm^2 for Case L/H. Similarly, the steady-state saltwater intrusion lengths showed variations: 38.99 cm for Case L, 39.78 cm for Case H, 41.76 cm for Case H/L, and 36.38 cm for Case L/H. Notably, the highest repulsion of saltwater intrusion was observed at an inclination angle of 76.0° for cutoff-wall depths up to a ratio of 0.623. However, as the depth ratio increased to 0.811, the maximum repulsion ratio was achieved at an angle of 63.4° across all four aquifers under investigation. This intriguingly demonstrated that an inclination angle of 63.4° had a more pronounced impact on reducing the extent of seawater intrusion compared to a vertical cutoff-wall (90.0° angle).

Additionally, an inclination angle of 45.0° for the cutoff-wall had a significant impact on the area covered by the saltwater wedge. This effect resulted in reductions of 79.54 cm^2 , 75.19 cm^2 , 79.74 cm^2 , and 95.0 cm^2 for Case L, Case H, Case H/L, and Case L/H, respectively. These measurements were taken at an inclined cutoff depth ratio of 0.811.

Future study should expand their scope to encompass a broader range of aquifer characteristics, including depth, breadth, and lateral extent, to build adaptable solutions for a variety of geological environments. Furthermore, research should explore various placements for inclined cutoff walls to fully understand their influence.

Appendix

Table A-1 Model parameters utilized in the numerical simulations

Parameter	Value	Unit
Aquifer length (L)	90	cm
Aquifer height (H)	30	cm
Freshwater head (h_f)	27.5	cm
Saltwater head (h_s)	26.5	cm
Freshwater density (ρ_f)	1000	g/L
Saltwater density (ρ_s)	1025	g/L
Salt concentration in freshwater (C_f)	0.0	g/L
Salt concentration in saltwater (C_s)	36.0	g/L
Investigated aquifer settings	Case L, Case H, Case H/L, Case L/H	-
Hydraulic conductivity (K_H) High K layer	0.700	cm/s
Hydraulic conductivity (K_L) Low K layer	0.377	cm/s
Porosity (n)	0.4	-
Longitudinal dispersivity (α_L)	0.15	cm
Transversal dispersivity (α_T)	0.015	cm
Specific yield (S_y)	0.2	-
Depth of cutoff-wall (H_c)	10, 15, 20, 25	cm
Cutoff-wall Inclination angle (θ)	45.00, 63.43, 75.96, 90.00, 104.04, 116.57, 135.00	degree
Hydraulic gradient (J)	1.11	%
Dimensionless cutoff-wall depth ($H_c^* = 1 - \frac{H-H_c}{h_s}$)	0.245, 0.434, 0.623, 0.811	-

Table A-2 Summary of the investigated cases for each aquifer

No.	Cutoff-wall Inclination angle (θ)	Cutoff-wall depth (H_c , cm)	Experimental	Numerical
1*	-	-	✓	✓
2	45.00°	10	-	✓
3		15	-	✓
4		20	-	✓
5		25	-	✓
6	63.43°	10	✓	✓
7		15	✓	✓
8		20	✓	✓
9		25	✓	✓
10	75.96°	10	-	✓
11		15	-	✓
12		20	-	✓
13		25	-	✓
14	90.00°	10	✓	✓
15		15	✓	✓
16		20	✓	✓
17		25	✓	✓

No.	Cutoff-wall Inclination angle (θ)	Cutoff-wall depth (H_c , cm)	Experimental	Numerical
18	104.04°	10	-	✓
19		15	-	✓
20		20	-	✓
21		25	-	✓
22		10	✓	✓
23	116.57°	15	✓	✓
24		20	✓	✓
25		25	✓	✓
26		10	-	✓
27	135.00°	15	-	✓
28		20	-	✓
29		25	-	✓

*Represent the base case of SWI where no countermeasures of SWI were utilized

Table A-3 Steady-state numerical results of Saltwater Intrusion wedge length for cutoff-wall depths of 10.0, 15.0, 20.0, and 25.0 cm at cutoff-wall inclination angles of 45.0°, 63.4°, 76.0°, 90.0°, 104.0°, 116.6°, and 135.0° for Case L, Case H, Case H/L, and Case L/H

		Numerical Saltwater Intrusion Wedge Length (cm)				
		Base Case	$H_c = 10$ cm	$H_c = 15$ cm	$H_c = 20$ cm	$H_c = 25$ cm
			$H_c^* = 0.245$	$H_c^* = 0.434$	$H_c^* = 0.623$	$H_c^* = 0.811$
Case L	$\theta = 45.0^\circ$	38.99	39.04	36.05	30.00	20.77
	$\theta = 63.4^\circ$		38.99	35.97	27.61	15.52
	$\theta = 76.0^\circ$		38.36	33.66	25.70	17.11
	$\theta = 90.0^\circ$		38.40	34.46	27.06	20.53
	$\theta = 104.0^\circ$		38.63	35.28	30.56	26.76
	$\theta = 116.6^\circ$		38.83	36.80	33.82	31.27
	$\theta = 135.0^\circ$		39.55	38.04	37.00	36.05
Case H	$\theta = 45.0^\circ$	39.87	38.99	35.97	30.00	20.77
	$\theta = 63.4^\circ$		38.83	34.54	26.42	15.28
	$\theta = 76.0^\circ$		38.08	33.50	25.62	17.12
	$\theta = 90.0^\circ$		38.04	33.58	26.58	20.29
	$\theta = 104.0^\circ$		38.99	35.57	30.64	26.66
	$\theta = 116.6^\circ$		38.99	36.53	33.58	31.27
	$\theta = 135.0^\circ$		39.47	38.04	37.00	36.13
Case H/L	$\theta = 45.0^\circ$	41.76	42.53	39.35	32.26	17.52
	$\theta = 63.4^\circ$		41.54	36.32	27.29	13.22
	$\theta = 76.0^\circ$		40.70	33.05	23.10	16.01
	$\theta = 90.0^\circ$		40.70	33.05	25.01	19.67
	$\theta = 104.0^\circ$		41.02	35.20	29.15	25.96
	$\theta = 116.6^\circ$		40.54	37.91	33.05	30.66
	$\theta = 135.0^\circ$		39.55	38.04	37.00	36.05

		Numerical Saltwater Intrusion Wedge Length (cm)				
		Base Case	$H_c = 10$ cm	$H_c = 15$ cm	$H_c = 20$ cm	$H_c = 25$ cm
			$H_c^* = 0.245$	$H_c^* = 0.434$	$H_c^* = 0.623$	$H_c^* = 0.811$
Case L/H	$\theta = 45.0^\circ$	36.38	36.00	33.53	29.55	23.42
	$\theta = 63.4^\circ$		36.00	33.10	28.51	17.20
	$\theta = 76.0^\circ$		35.79	33.05	27.16	18.24
	$\theta = 90.0^\circ$		35.36	33.05	28.04	21.11
	$\theta = 104.0^\circ$		36.08	34.41	31.38	27.48
	$\theta = 116.6^\circ$		36.16	34.85	33.26	31.43
	$\theta = 135.0^\circ$		36.56	35.76	35.20	35.04

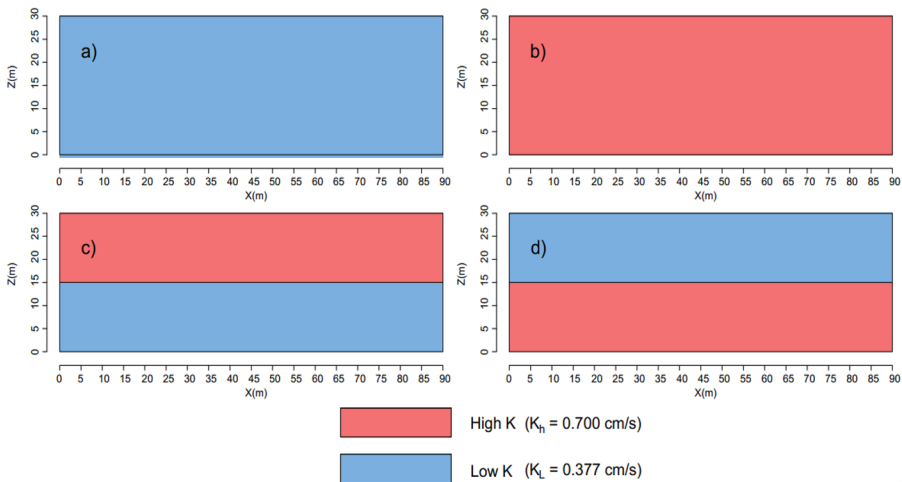


Fig. A-2 Schematic design of the investigated aquifer settings: **a** homogeneous High K, **b** homogeneous Low K, **c** stratified H/L, and **d** stratified L/H

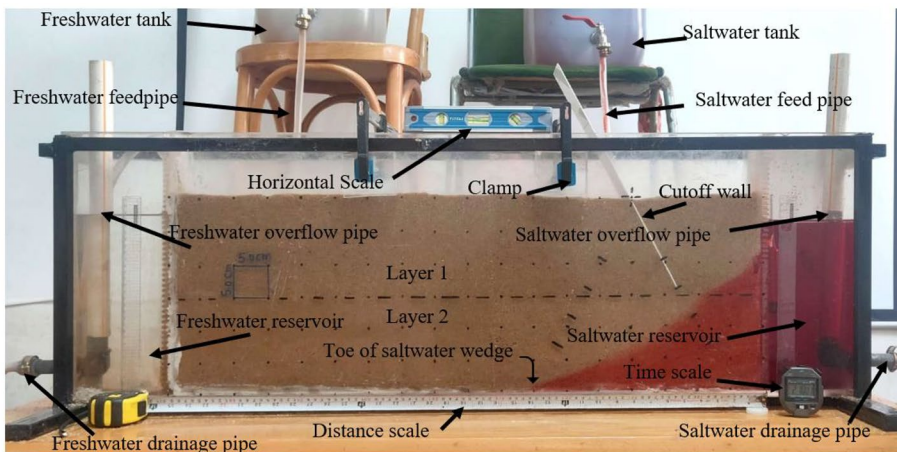


Fig. A-1 Photograph of the experimental setup

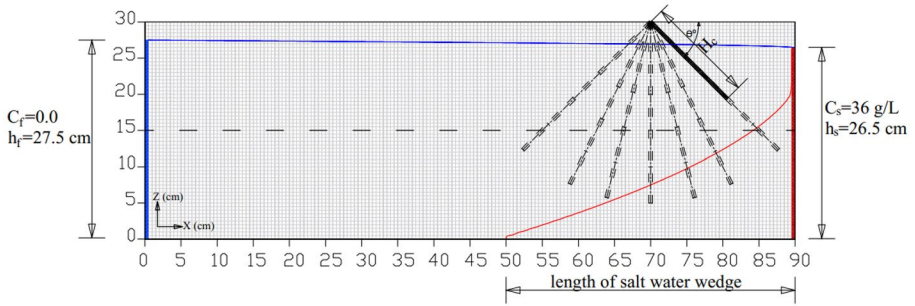


Fig. A-3 Boundary conditions for the numerical simulations



Fig. A-4 Experimental results of saltwater intrusion wedge for $\theta = 90^\circ$, for various aquifer cases a Case L, b Case H, c case H/L, and d Case L/H, for four various presented cutoff-wall depths

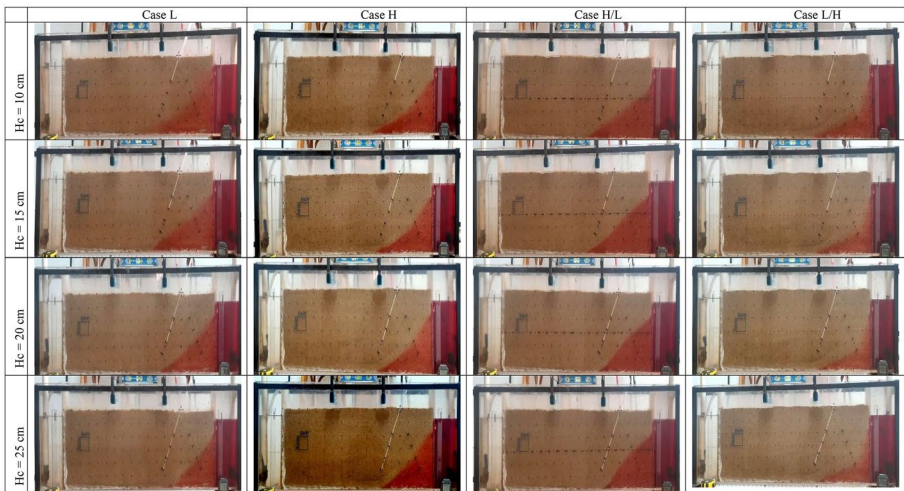


Fig. A-5 Experimental results of saltwater intrusion wedge for $\theta = 116.6^\circ$, for various aquifer cases a Case L, b Case H, c Case H/L, and d Case L/H, for four various presented cutoff-wall depths

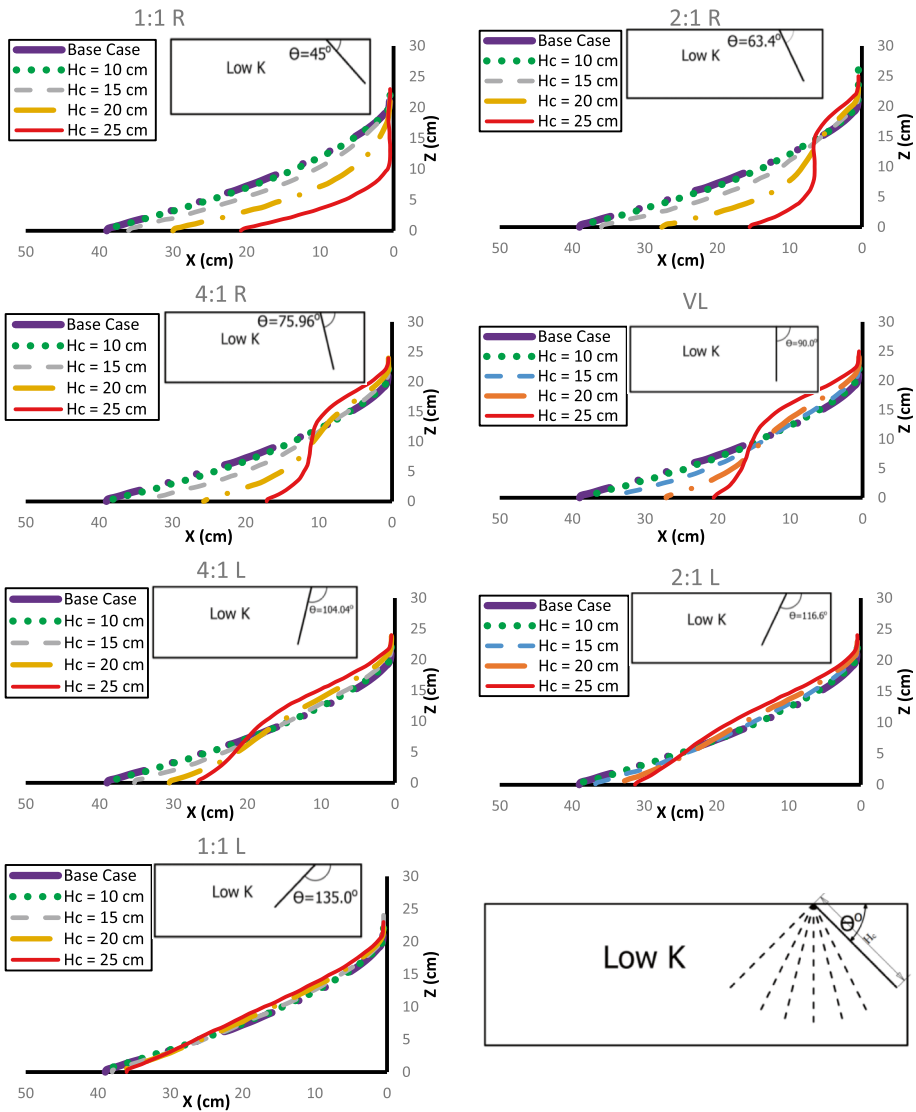


Fig. A-6 Steady-state numerical results of saltwater intrusion wedge for cutoff-wall depths of 10.0, 15.0, 20.0, and 25.0 cm at cutoff-wall inclination angles of 45.0°, 63.4°, 76.0°, 90.0°, 104.0°, 116.6°, and 135.0° for a homogenous low conductivity aquifer (Case L)

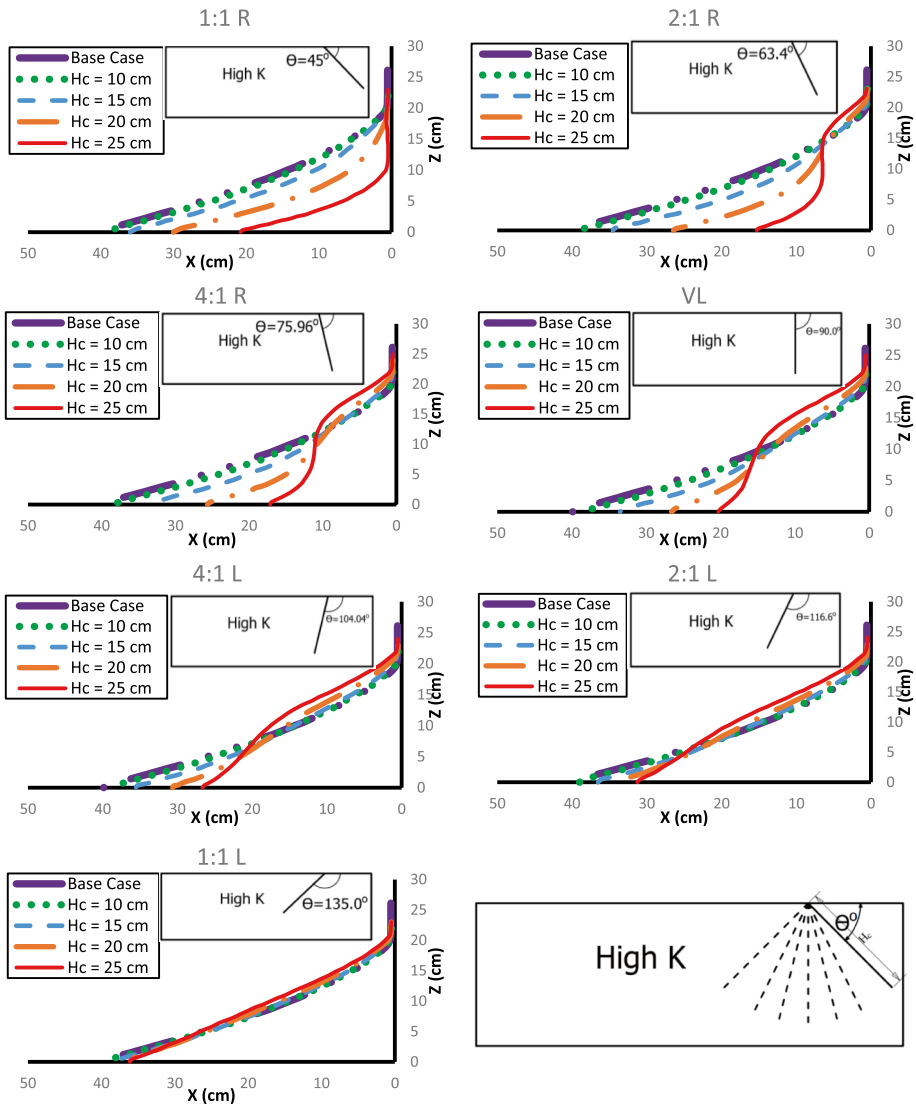


Fig. A-7 Steady-state numerical results of saltwater intrusion wedge for cutoff-wall depths of 10.0, 15.0, 20.0, and 25.0 cm at cutoff-wall inclination angles of 45.0°, 63.4°, 76.0°, 90.0°, 104.0°, 116.6°, and 135.0° for a homogenous High conductivity aquifer (Case H)

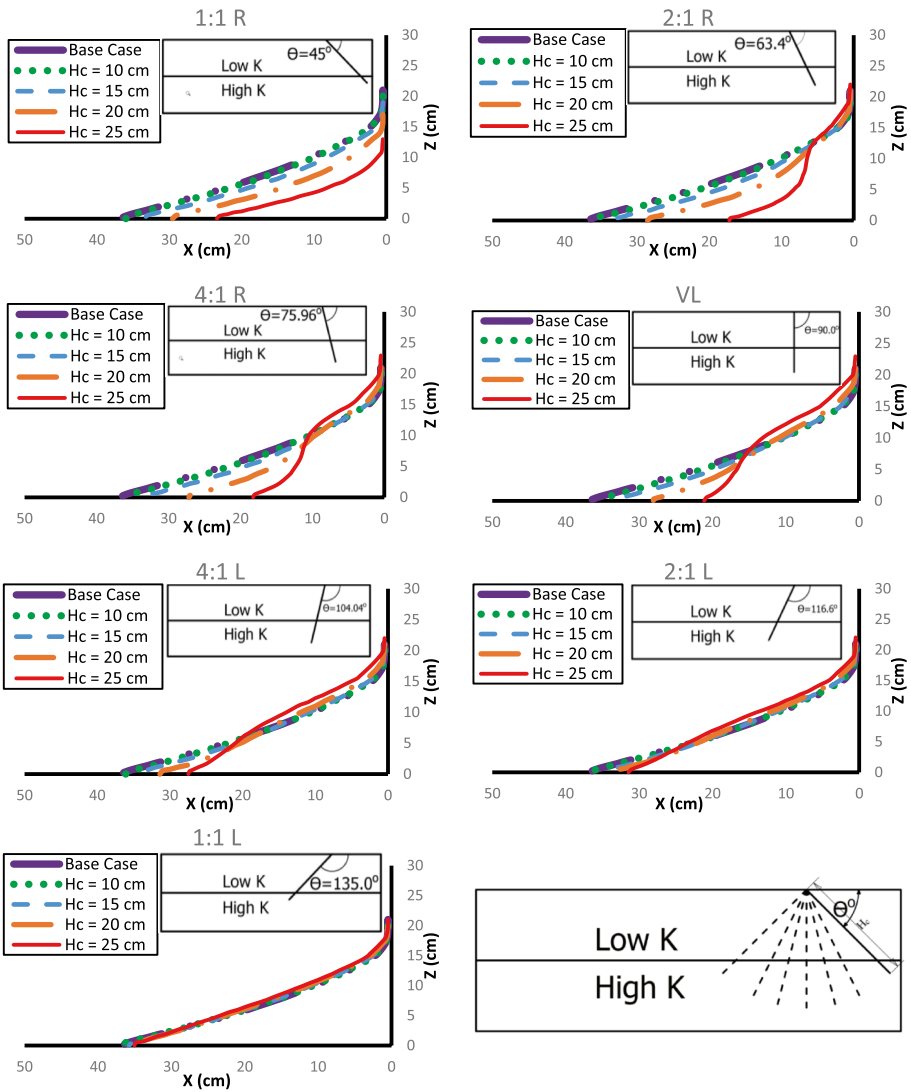


Fig. A-8 Steady-state numerical results of saltwater intrusion wedge for cutoff-wall depths of 10.0, 15.0, 20.0, and 25.0 cm at cutoff-wall inclination angles of 45.0°, 63.4°, 76.0°, 90.0°, 104.0°, 116.6°, and 135.0° for a stratified aquifer with a high conductivity layer below a low conductivity layer (Case L/H)

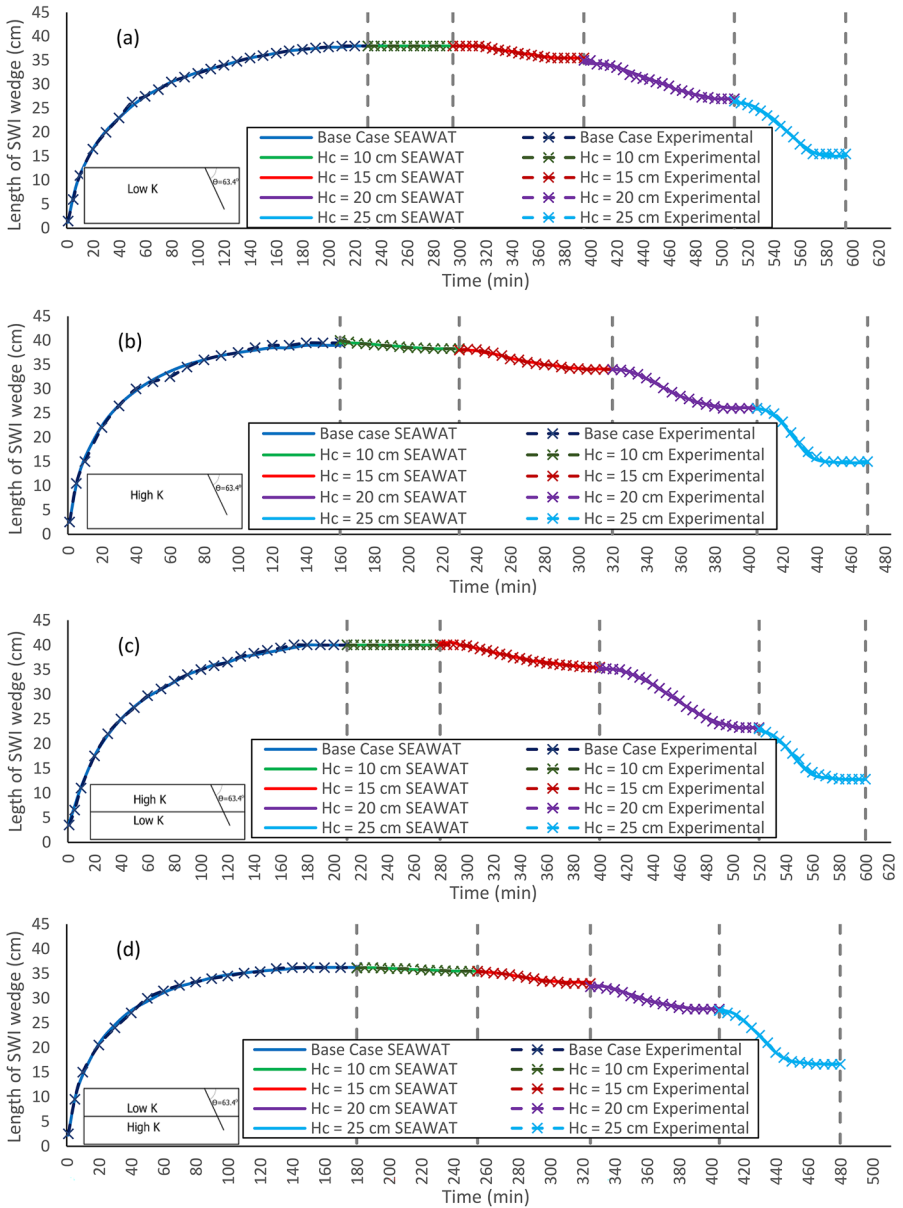


Fig. A-9 Comparison between the experimental and numerical SWI lengths for Case L (a), Case H (b), Case H/L (c), and Case L/H (d) with cutoff-wall inclination angle $\theta = 63.4^\circ$

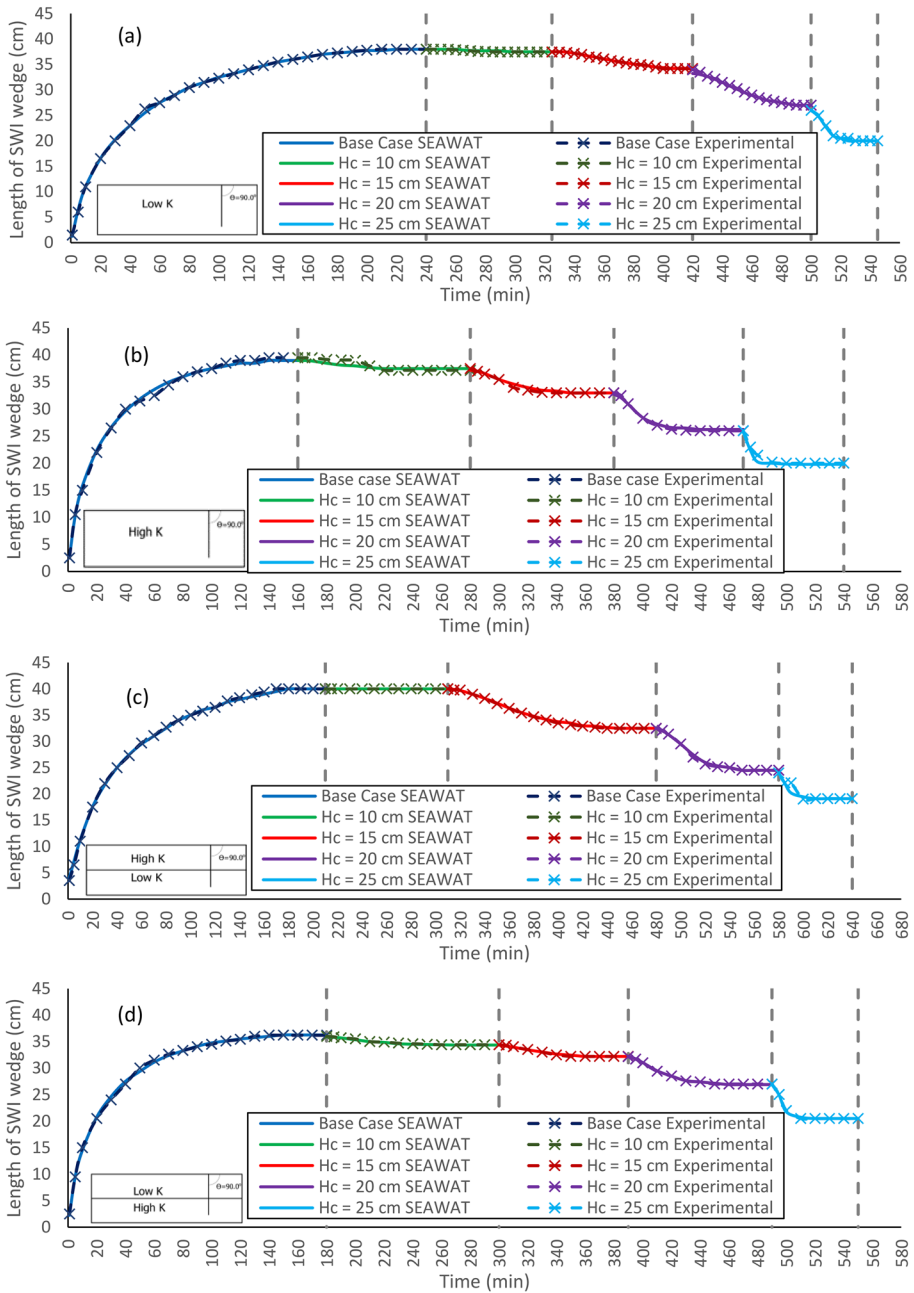


Fig. A-10 Comparison between the experimental and numerical SWI lengths for Case L (a), Case H.(b), Case H/L.(c), and Case L/H.(d) with cutoff-wall inclination angle $\theta = 90.0^\circ$

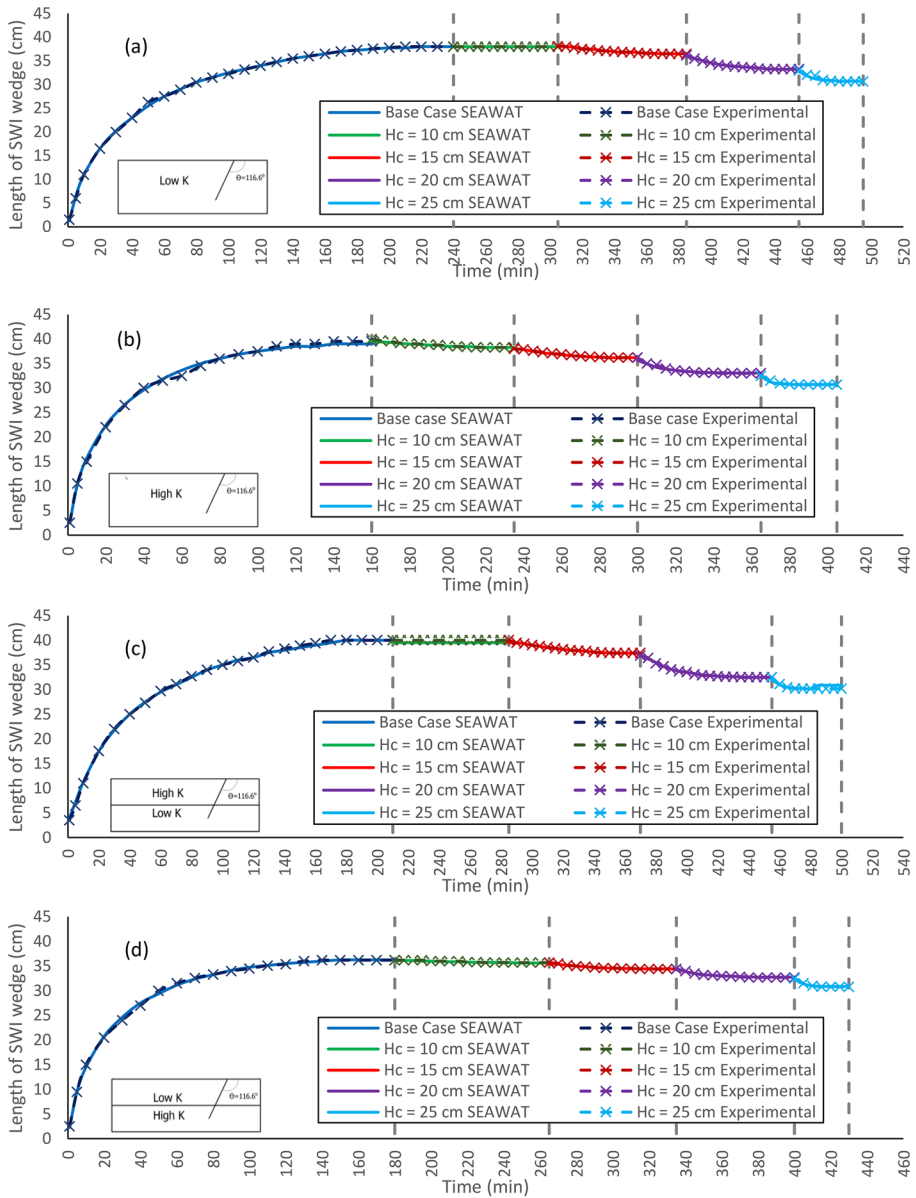


Fig. A-11 Comparison between the experimental and numerical SWI lengths for Case L (a), Case H (b), Case H/L (c), and Case L/H (d) with cutoff-wall inclination angle $\theta=116.6^\circ$

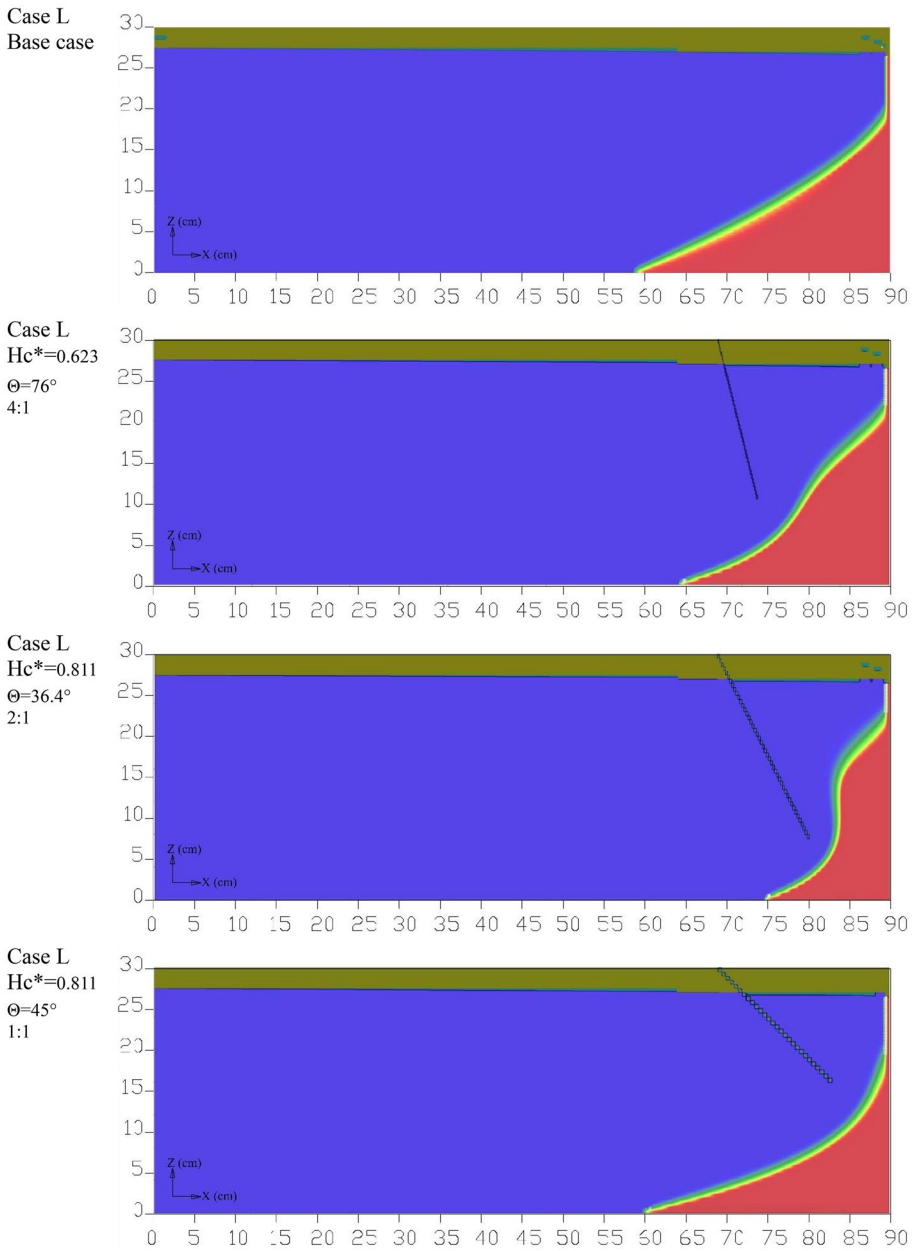


Fig. A-12 Pictures of the modelling results for case L

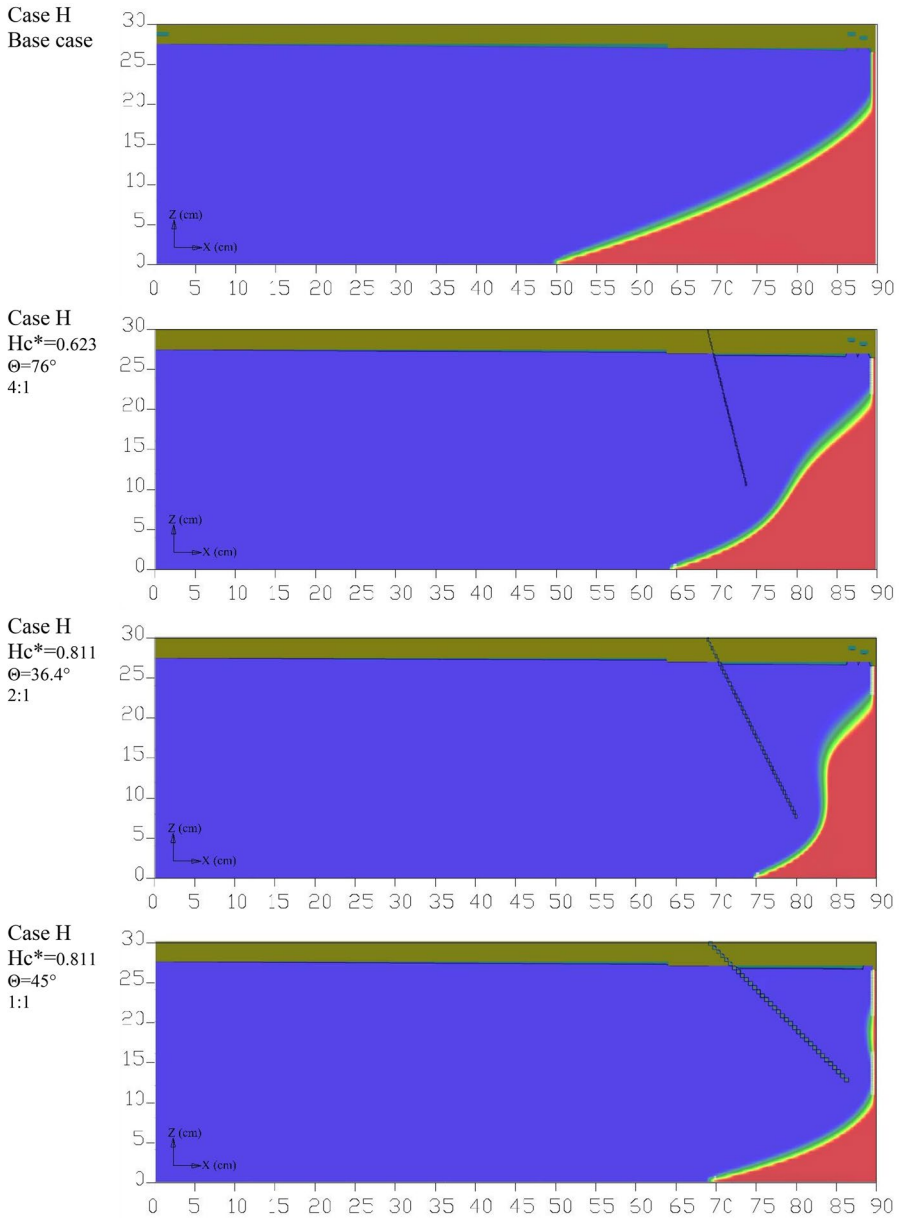


Fig. A-13 Pictures of the modelling results for case H

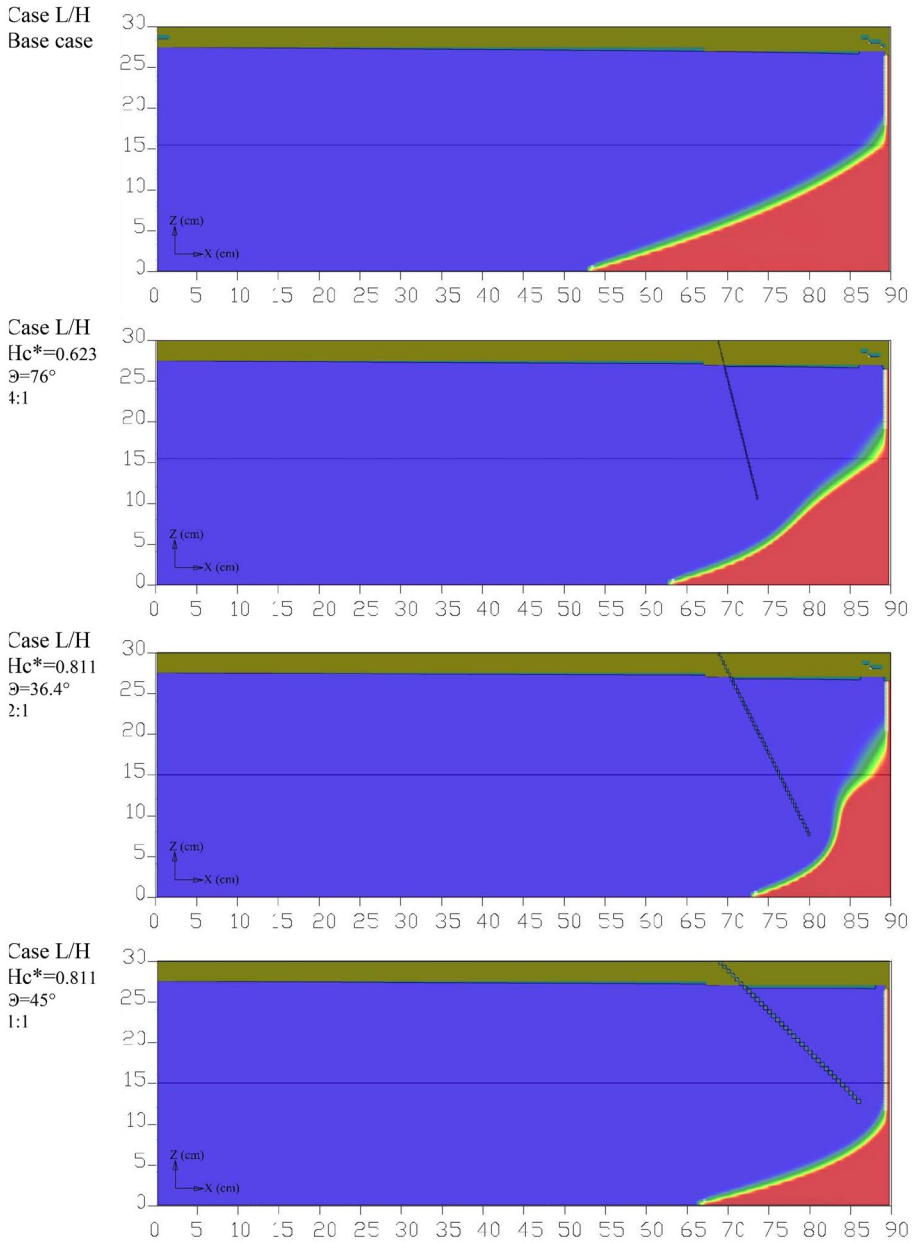


Fig. A-14 Pictures of the modelling results for case L/H

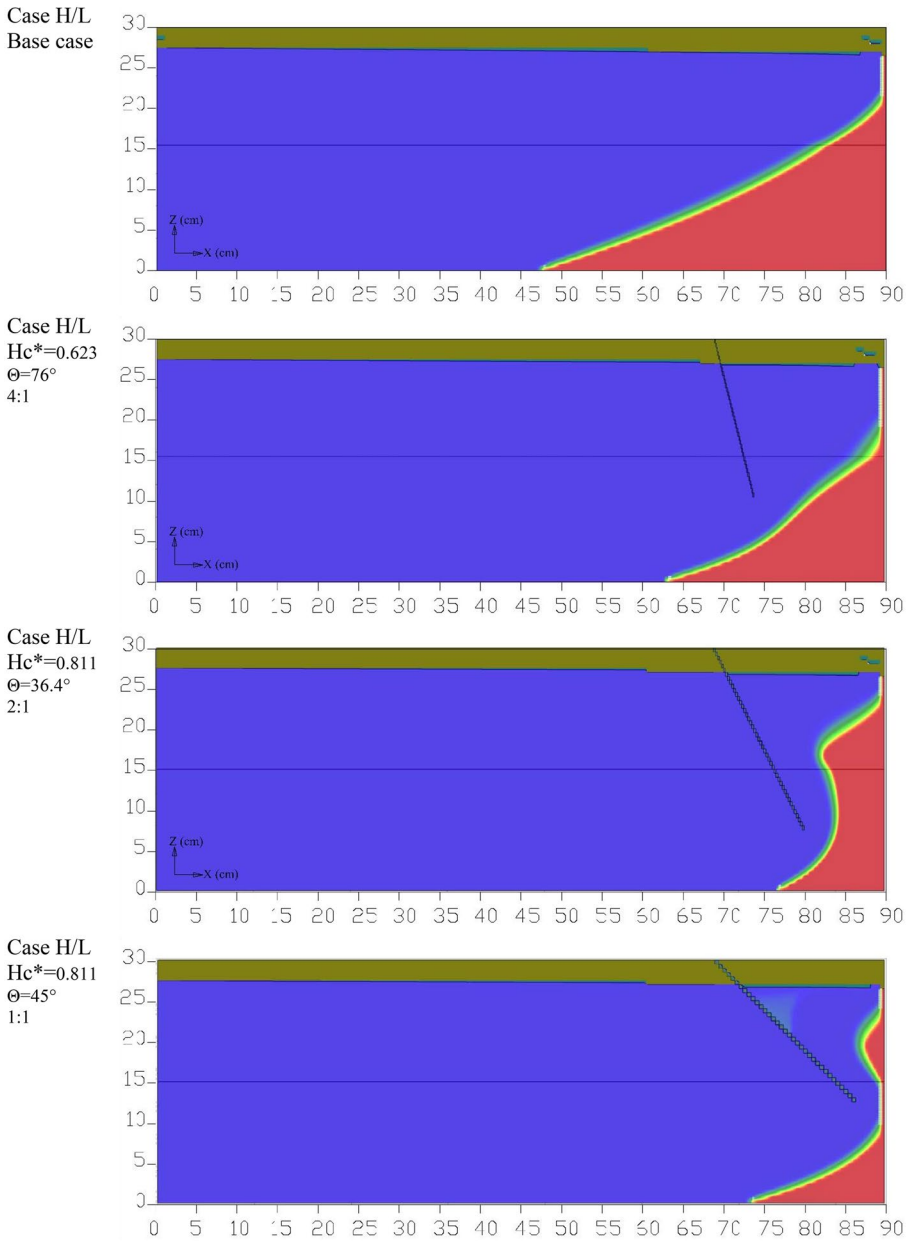


Fig. A-15 Pictures of the modelling results for case H/L

Author Contributions This paper originated as a part of the PhD thesis of the first author (Sobhy R. Emara) under the supervision of Asaad M. Armanuos, Tamer A. Gado, and Bakenaz A. Zeidan. All authors contributed to the study conception and design. Sobhy R. Emara and Asaad M. Armanuos carried out the experiments. Sobhy R. Emara carried out the simulations. All authors contributed to the interpretation of the results. The first draft of the manuscript was written by Sobhy R. Emara. And all authors commented on previous versions of the manuscript.

Funding Open access funding provided by The Science, Technology & Innovation Funding Authority (STDF) in cooperation with The Egyptian Knowledge Bank (EKB). The authors declare that no funds, grants, or other support were received during the preparation of this manuscript.

Availability of Data and Materials The corresponding author can provide the data that back up the study's conclusions upon request.

Declarations

Ethical Approval All authors read and approved the final manuscript.

Competing Interests The authors have no relevant financial or non-financial interests to disclose.

Open Access This article is licensed under a Creative Commons Attribution 4.0 International License, which permits use, sharing, adaptation, distribution and reproduction in any medium or format, as long as you give appropriate credit to the original author(s) and the source, provide a link to the Creative Commons licence, and indicate if changes were made. The images or other third party material in this article are included in the article's Creative Commons licence, unless indicated otherwise in a credit line to the material. If material is not included in the article's Creative Commons licence and your intended use is not permitted by statutory regulation or exceeds the permitted use, you will need to obtain permission directly from the copyright holder. To view a copy of this licence, visit <http://creativecommons.org/licenses/by/4.0/>.

References

- Abarca E, Clement TP (2009) A novel approach for characterizing the mixing zone of a saltwater wedge. *Geophys Res Lett* 36. <https://doi.org/10.1029/2008GL036995>
- Abd-Elaty I, Abd-Elhamid HF, Nezhad MM (2019) Numerical analysis of physical barriers systems efficiency in controlling saltwater intrusion in coastal aquifers. *Environ Sci Pollut Res* 26:35882–35899. <https://doi.org/10.1007/s11356-019-06725-3>
- Abd-Elaty I, Pugliese L, Straface S (2022) Inclined physical subsurface barriers for saltwater intrusion management in coastal aquifers. *Water Resour Manag* 36:2973–2987. <https://doi.org/10.1007/s11269-022-03156-7>
- Abdoulhalik A, Abdelgawad AM, Ahmed AA et al (2022a) Assessing the protective effect of cutoff walls on groundwater pumping against saltwater upconing in coastal aquifers. *J Environ Manag* 323:116200. <https://doi.org/10.1016/j.jenvman.2022.116200>
- Abdoulhalik A, Ahmed A, Abdelgawad A, Hamill G (2022b) The impact of a low-permeability upper layer on transient seawater intrusion in coastal aquifers. *J Environ Manag* 307:114602. <https://doi.org/10.1016/j.jenvman.2022.114602>
- Abdoulhalik A, Ahmed AA (2017) The effectiveness of cutoff walls to control saltwater intrusion in multi-layered coastal aquifers: Experimental and numerical study. *J Environ Manag* 199:62–73. <https://doi.org/10.1016/j.jenvman.2017.05.040>
- Ahmed A, Robinson G, Hamill G, Etsias G (2022) Seawater intrusion in extremely heterogeneous laboratory-scale aquifer: Steady-state results. *Water* 14:1069. <https://doi.org/10.3390/w14071069>
- Armanuos AM, Al-Ansari N, Yaseen ZM (2020a) Assessing the effectiveness of using recharge wells for controlling the saltwater intrusion in unconfined coastal aquifers with sloping beds: Numerical study. *Sustainability* 12:2685. <https://doi.org/10.3390/su12072685>
- Armanuos AM, Al-Ansari N, Yaseen ZM (2020b) Underground barrier wall evaluation for controlling saltwater intrusion in sloping unconfined coastal aquifers. *Water* 12:2403. <https://doi.org/10.3390/w12092403>
- Armanuos AM, Ibrahim MG, Mahmud WE et al (2019) Analysing the combined effect of barrier wall and freshwater injection countermeasures on controlling saltwater intrusion in unconfined coastal aquifer systems. *Water Resour Manag* 33:1265–1280. <https://doi.org/10.1007/s11269-019-2184-9>
- Brakefield L (2008) Physical and numerical modeling of buoyant groundwater plumes. Auburn University, Thesis

- Chang Q, Zheng T, Chen Y et al (2020) Investigation of the elevation of saltwater wedge due to subsurface dams. *Hydrol Process* 34:4251–4261. <https://doi.org/10.1002/hyp.13863>
- Chang Q, Zheng T, Gao C et al (2022) How to cope with downstream groundwater deterioration induced by cutoff walls in coastal aquifers. *J Hydrol* 610:127804. <https://doi.org/10.1016/j.jhydrol.2022.127804>
- Chang Q, Zheng T, Zheng X et al (2019) Effect of subsurface dams on saltwater intrusion and fresh groundwater discharge. *J Hydrol* 576:508–519. <https://doi.org/10.1016/j.jhydrol.2019.06.060>
- Chang SW, Clement TP (2012) Experimental and numerical investigation of saltwater intrusion dynamics in flux-controlled groundwater systems. *Water Resour Res* 48. <https://doi.org/10.1029/2012WR012134>
- Christensen BA, Evans AJ Jr (1974) A physical model for prediction and control of saltwater intrusion in the Floridan aquifer. University of Florida, Water Resour Res Cent Gainesv Fa, p 88
- Dagan G, Zeitoun DG (1998) Seawater-freshwater interface in a stratified aquifer of random permeability distribution. *J Contam Hydrol* 29:185–203. [https://doi.org/10.1016/S0169-7722\(97\)00013-2](https://doi.org/10.1016/S0169-7722(97)00013-2)
- Fan Y, Lu W, Miao T et al (2020) Multiobjective optimization of the groundwater exploitation layout in coastal areas based on multiple surrogate models. *Environ Sci Pollut Res* 27:19561–19576. <https://doi.org/10.1007/s11356-020-08367-2>
- Gao M, Zheng T, Chang Q et al (2021) Effects of mixed physical barrier on residual saltwater removal and groundwater discharge in coastal aquifers. *Hydrol Process* 35. <https://doi.org/10.1002/hyp.14263>
- Houben GJ, Stoeckl L, Mariner KE, Choudhury AS (2018) The influence of heterogeneity on coastal groundwater flow - physical and numerical modeling of fringing reefs, dykes and structured conductivity fields. *Adv Water Resour* 113:155–166. <https://doi.org/10.1016/j.advwatres.2017.11.024>
- Hussain MS, Abd-Elhamid HF, Javadi AA, Sherif MM (2019) Management of Seawater Intrusion in Coastal Aquifers: A Review. *Water* 11:2467. <https://doi.org/10.3390/w11122467>
- Hussain MS, Javadi A, Sherif M (2016) Artificial recharge of coastal aquifers using treated wastewater to control saltwater intrusion. *Qual Quant* 1:4. <https://doi.org/10.13140/RG.2.1.2285.9920>
- Jamshidzadeh Z, Ghasemzadeh H (2017) The effects of cut-off walls on repulsing saltwater based on modeling of density-driven groundwater flow and salt transport. *Numer Methods Civ Eng* 1:45–53. <https://doi.org/10.29252/nmce.1.4.45>
- Javadi A, Hussain M, Sherif M, Farmani R (2015) Multi-objective optimization of different management scenarios to control seawater intrusion in coastal aquifers. *Water Resour Manag* 29:1843–1857. <https://doi.org/10.1007/s11269-015-0914-1>
- Kaleris VK, Ziogas AI (2013) The effect of cutoff walls on saltwater intrusion and groundwater extraction in coastal aquifers. *J Hydrol* 476:370–383. <https://doi.org/10.1016/j.jhydrol.2012.11.007>
- Lee W-D, Yoo Y-J, Jeong Y-M, Hur D-S (2019) Experimental and numerical analysis on hydraulic characteristics of coastal aquifers with seawall. *Water* 11:2343. <https://doi.org/10.3390/w11112343>
- Li F, Chen X, Liu C et al (2018) Laboratory tests and numerical simulations on the impact of subsurface barriers to saltwater intrusion. *Nat Hazards* 91:1223–1235. <https://doi.org/10.1007/s11069-018-3176-4>
- Liu Y, Shen M, Zhao J et al (2019) A new optimization method for the layout of pumping wells in oases: Application in the Qira Oasis, Northwest China. *Water* 11:970. <https://doi.org/10.3390/w11050970>
- Lu C, Chen Y, Zhang C, Luo J (2013) Steady-state freshwater–seawater mixing zone in stratified coastal aquifers. *J Hydrol* 505:24–34. <https://doi.org/10.1016/j.jhydrol.2013.09.017>
- Luyun R Jr, Momii K, Nakagawa K (2009) Laboratory-scale saltwater behavior due to subsurface cutoff wall. *J Hydrol* 377:227–236. <https://doi.org/10.1111/j.1745-6584.2010.00719.x>
- Luyun R, Momii K, Nakagawa K (2011) Effects of recharge wells and flow barriers on seawater intrusion. *Ground Water* 49:239–249. <https://doi.org/10.1111/j.1745-6584.2010.00719.x>
- Mehdizadeh SS, Badaruddin S, Khatibi S (2019) Abstraction, desalination and recharge method to control seawater intrusion into unconfined coastal aquifers. *Glob J Environ Sci Manag* 5. <https://doi.org/10.22034/gjesm.2019.01.09>
- Motallebian M, Ahmadi H, Raouf A, Cartwright N (2019) An alternative approach to control saltwater intrusion in coastal aquifers using a freshwater surface recharge canal. *J Contam Hydrol* 222:56–64. <https://doi.org/10.1016/j.jconhyd.2019.02.007>
- Ranjbar A, Mahjouri N, Cherubini C (2020) Development of an efficient conjunctive meta-model-based decision-making framework for saltwater intrusion management in coastal aquifers. *J Hydro-Environ Res* 29:45–58. <https://doi.org/10.1016/j.jher.2019.11.005>
- Sun Q, Zheng T, Zheng X et al (2019) Influence of a subsurface cut-off wall on nitrate contamination in an unconfined aquifer. *J Hydrol* 575:234–243. <https://doi.org/10.1016/j.jhydrol.2019.05.030>
- Takahashi M, Momii K, Luyun R (2018) Laboratory scale investigation of dispersion effects on saltwater movement due to cutoff wall installation. *E3S Web Conf* 54:00038. <https://doi.org/10.1051/e3sconf/20185400038>
- Vats OP, Sharma B, Stamm J, Bhattacharjya RK (2020) Groundwater circulation well for controlling saltwater intrusion in coastal aquifers: Numerical study with experimental validation. *Water Resour Manag* 34:3551–3563. <https://doi.org/10.1007/s11269-020-02635-z>

- Voss CI, Souza WR (1987) Variable density flow and solute transport simulation of regional aquifers containing a narrow freshwater-saltwater transition zone. *Water Resour Res* 23:1851–1866. <https://doi.org/10.1029/WR023i010p01851>
- Walther M, Graf T, Kolditz O et al (2017) How significant is the slope of the sea-side boundary for modelling seawater intrusion in coastal aquifers? *J Hydrol* 551:648–659. <https://doi.org/10.1016/j.jhydrol.2017.02.031>
- Werner AD, Bakker M, Post VEA et al (2013) Seawater intrusion processes, investigation and management: Recent advances and future challenges. *Adv Water Resour* 51:3–26. <https://doi.org/10.1016/j.advwatres.2012.03.004>
- Wu H, Lu C, Kong J, Werner AD (2020) Preventing seawater intrusion and enhancing safe extraction using finite-length, impermeable subsurface barriers: 3D analysis. *Water Resour Res* 56. <https://doi.org/10.1029/2020WR027792>
- Zheng H, Wenxi L, Yue F et al (2021) Optimal location of cutoff walls for seawater intrusion. *Appl Water Sci* 11:179. <https://doi.org/10.1007/s13201-021-01514-1>
- Zheng T, Gao M, Chang Q et al (2022) Dynamic desalination of intruding seawater after construction of cut-off walls in a coastal unconfined aquifer. *Front Mar Sci* 9:857807. <https://doi.org/10.3389/fmars.2022.857807>
- Zheng T, Zheng X, Chang Q et al (2021) Timescale and effectiveness of residual saltwater desalinization behind subsurface dams in an unconfined aquifer. *Water Resour Res* 57:e2020WR028493. <https://doi.org/10.1029/2020WR028493>

Publisher's Note Springer Nature remains neutral with regard to jurisdictional claims in published maps and institutional affiliations.